Comparison of One Dimensional and Two Dimensional Population Balance Model for Optimization of a Crystallization Process

Tamar Rosenbaum,[†] Victoria Mbachu,[†] Niall Mitchell,[§] John Gamble,[£] Patricia Cho,[‡] and Joshua Engstrom[†]*

[†] Drug Product Science and Technology, Bristol-Myers Squibb, 1 Squibb Drive, New Brunswick NJ 08903

[£] Drug Product Science and Technology, Bristol-Myers Squibb, Moreton UK

[‡] Chemical and Synthetic Development, Bristol-Myers Squibb, 1 Squibb Drive, New Brunswick, NJ 08903

§ Process Systems Enterprise (PSE) – A Siemens Business, 6th Floor East, 26-28 Hammersmith Grove, London UK W6 7HA

ABSTRACT: In this work, the advantage of two-dimensional population balance modeling (2D PBM) for a needle-shaped API is highlighted by comparing the one-dimensional population balance model (1D PBM) developed for an antisolvent crystallization with the 2D PBM. The API utilized for this work had extremely slow desupersaturation, and was not able to achieve solubility concentration despite a ~50 h seed bed age. While the 1D PBM is useful in optimizing the crystallization process to enhance desupersaturation, it is unable to match the particle size quantiles well. 2D PBM was necessary to probe the impact of crystallization process parameters on particle aspect ratio (AR). Simulations utilizing the 2D PBM indicated that regardless of antisolvent addition rate or seed morphology, the final material would still be high aspect ratio. This knowledge saved the investment of much time and efforts in trying to minimize particle AR with changes in crystallization processing parameters alone.

KEY WORDS: crystallization, population balance, process modelling, crystal morphology

INTRODUCTION:

Crystallization is the preferred method for isolating an active pharmaceutical ingredient (API) from the reaction stream.[1, 2] The crystallization step is very important, because it is responsible for controlling the API purity, physical form, particle size distribution (PSD) and particle morphology. Therefore, significant time, labor, and materials are invested to study the many process parameters within the crystallization step, such as temperature, agitation rate, seed load, antisolvent addition rate and cooling rate, to determine their impact on the isolated API.[1] However, the results from lab scale experiments may not be indicative of the behavior when the crystallization is run at larger scales, due differences in parameter scaling.[3] Understanding fundamental crystallization kinetics can provide a more robust method to design and optimize the crystallization process to consistently generate material with similar PSD and morphology.[1] Although direct experimental measurement of the crystallization kinetics is typically too time consuming to render feasible,[4] modelling of the crystallization process can be utilized to provide insight into the kinetics.[1, 2, 4]

The crystallization process involves formation of nuclei from solution, and the subsequent growth of those nuclei throughout various stages of the process.[5] Therefore, the crystallization process is well-suited for population balance modeling (PBM), which utilizes a set of differential algebraic equations to describe the temporal evolution of the distribution of a given particle property, such as PSD.[6] Advances in both analytical equipment and computational methods have allowed PBM to become more increasingly accessible to the crystallization community.[7] Typically, PBM of the crystallization process has been conducted by utilizing a single dimension to describe the particle size, representing the particles as spheres.[8] While this simplification may work well for low aspect ratio particles, a one-dimensional PBM can have difficulty predicting crystallization behavior for high aspect ratio particles such as needles. The latest numerical and

computational advancements have allowed for the solving of 2D PBMs, which are able to fulfill this opportunity.[8, 9]

The difficulty of solving the multi-dimensional differential algebraic equations associated with two-dimensional PBM had previously precluded broader application of these models.[8, 10] Recent enhancements in numerical techniques that allow for the existence of analytical solutions has brought two-dimensional PBM to a state of practical application.[11] Although many APIs crystallize in needle or rod-like morphologies, multidimensional PBM of the crystallization process is still under-utilized. This is reflected in the relatively few published multidimensional crystallization PBMs,[9, 12-22] in comparison with the more prevalently published one-dimensional PBMs[23-40].

To highlight the benefits of 2D PBM, we compare a one-dimensional PBM and a two-dimensional PBM that were developed for an isothermal antisolvent crystallization process of a needle-shaped API. The API exhibited extremely slow desupersaturation from the supernatant and did not reach full desupersaturation even after a fifty hour seed age. The capabilities of both models for guiding the lab scale experiments, albeit in different capacities, are presented in this work.

METHODS

Materials: The API used for all experiments was BMS compound A, produced by BMS (New Brunswick, NJ). Reagent grade THF and acetone were purchased from Sigma-Aldrich (St. Louis, MO) and used as-is. HPLC grade acetonitrile was purchased from Sigma-Aldrich and used as-is.

Solubility Measurements: A stock solution of 1:1 THF:acetone v:v was prepared, and then various ratios of the stock solution with water (antisolvent) were prepared. The API and THF:acetone/water solution was added to a glass vial with a magnetic stir bar, such that there was excess solids present. The vial was stirred for 24 h at 20 ℃ on a stir plate equipped with temperature control. The supernatant was then filtered, diluted with acetonitrile, and run on HPLC (Shimadzu Scientific Instruments, Columbia MD). An HPLC calibration model was built with standards of known concentrations measured on the basis of mg of API/mL of solvent. In order to accommodate the mass balance requirement for model building, these values were converted from mg of API/mL of solvent to kg of API/kg of solution by assuming that the density of the mixture was a ratio of the densities of the individual solvents based on the solvent molar percent of the composition. The converted values were imported into gPROMS FormulatedProducts Utilities (gFP) version 1.5 (Process Systems Enterprise (PSE) Ltd., London UK) for parameter estimation of the solubility map across varying solvent compositions, treating the 1:1 THF:acetone mixture as a single entity, since the ratio of these two solvents was invariant for the experimental conditions studied in this work. Although the form of the solids was not checked, polymorph screening work (data not shown here) indicated that the input form is the most stable form across the solvent and temperature composition investigated, and no form change was observed in these solvent compositions across the temperature range considered for process design.

Crystallization Experiments: Experiments 1-3 were utilized to build the process models (1D and 2D), and experiments 4-8 were conducted to verify model predictions. Experiments 1 and 6 were run in a 250 mL Chemglass reactor (Chemglass, Vineland, NJ) with a half-moon impeller. Experiments 2, 3, and 8 were run in a 100 mL EasyMax reactor (Mettlar Toledo) with a pitched

blade turbine. Experiments 4, 5, and 7 were run in 100 mL Chemglass reactor with a half-moon impeller. Experiments 1, 2, 4, 6, and 8 utilized the same lot of seed material ("as-is" needles; D10 = 20 μm, D50 = 56 μm, D90 = 150 μm), and experiments 3, 5, and 7 utilized a micronized seed lot (D10 = 2 μm, D50 = 6 μm, D90 = 15 μm). All crystallization experiments were conducted at 20 °C. At varying time points during each crystallization experiment, supernatant samples were removed from the reactor, filtered and immediately diluted for HPLC concentration measurements (see "Desupersaturation Measurements" section below).

Table 1. Summary of crystallization experiments and conditions

Experiment	Reactor	API (g)	Agitation Rate (RPM)	Seed type	Seed Load (wt %)	Solvent: antisolvent ratio at seeding
1	250 mL Chemglass	9.44	350	As-is	2	2.32
2	100 mL EasyMax	5	350	As-is	2	2.7
3	100 mL EasyMax	5	350	micronized	2	2.7
4	100 mL Chemglass	4.72	550	As-is	2	2.32
5	100 mL	4.72	350	micronized	10	2.32

	Chemglass					
6	250 mL Chemglass	5	350	As-is	2	1.79
7	100 mL Chemglass	4.72	350	micronized	25	2.32
8	100 mL EasyMax	7	350	As-is	1	2.32

Experiment 1: 9.44 g of Compound A was charged into the reactor and dissolved in 50 mL THF and 50 mL acetone under 350 RPM agitation. 43 mL of water was charged to induce supersaturation. 198.4 mg of seeds was charged, and a slurry formed. The slurry was agitated for 21.5 h, after which 80.2 mL of water was added over 6 h. The slurry was isolated on a Buchner funnel, washed with 47.2 mL of 2:3 v:v acetone:water mix, and dried overnight at 70 ℃ in a vacuum oven.

Experiment 2: 5 g of Compound A was dissolved in 25 mL THF and 25 mL acetone under 350 RPM agitation. 18.5 mL water was added to induce supersaturation, and 100 mg seeds were added. The resulting slurry was aged over ~50 h, after which 40 mL of water was charged over 6 h. The slurry was isolated on a Buchner funnel, washed with 47.2 mL of 2:3 v:v acetone:water mix, and dried overnight at 70 ℃ in a vacuum oven.

Experiment 3: 5 g of Compound A was dissolved in 25 mL THF and 25 mL acetone under 350 RPM agitation. 18.5 mL water was added to induce supersaturation, and 100 mg seeds were added. The resulting slurry was aged over ~50 h, after which 40 mL of water was charged over

6 h. The slurry was isolated on a Buchner funnel, washed with 47.2 mL of 2:3 v:v acetone:water mix, and dried overnight at 70 ℃ in a vacuum oven.

Experiment 4: 4.72 g of Compound A was dissolved in 25 mL THF and 25 mL acetone under 550 RPM agitation. 21.5 mL of water was charged to generate supersaturation, and 94.4 mg seeds was added. The resulting slurry was aged for 24 h, after which 40 mL of water was charged over 6 h. The slurry was isolated on a Buchner funnel, washed with 47.2 mL of 2:3 v:v acetone:water mix, and dried overnight at 70 ℃ in a vacuum oven.

Experiment 5: 4.72 g of Compound A was dissolved in 25 mL THF and 25 mL acetone under 350 RPM agitation. 21.5 mL of water was charged to generate supersaturation, and 472 mg seeds was added. The resulting slurry was aged for 24 h, after which 40 mL of water was charged over 6 h. The slurry was isolated on a Buchner funnel, washed with 47.2 mL of 2:3 v:v acetone:water mix, and dried overnight at 70 ℃ in a vacuum oven.

Experiment 6: 5 g of Compound A was dissolved in 22.4 mL THF and 22.4 mL acetone under 350 RPM agitation. 25 mL water was added to induce supersaturation, and 100 mg seeds were added. The resulting slurry was aged over ~24 h, after which 40 mL of water was charged over 6 h. The slurry was isolated on a Buchner funnel, washed with 47.2 mL of 2:3 v:v acetone:water mix, and dried overnight at 70 ℃ in a vacuum oven.

Experiment 7: 4.72 g of Compound A was dissolved in 25 mL THF and 25 mL acetone under 350 RPM agitation. 21.5 mL of water was charged to generate supersaturation, and 1.1775 g seeds was added. The resulting slurry was aged for 3 h, after which 40 mL of water was charged over 6 h. The slurry was isolated on a Buchner funnel, washed with 47.2 mL of 2:3 v:v acetone:water mix, and dried overnight at 70 ℃ in a vacuum oven.

Experiment 8: 7 g of Compound A was dissolved in 37.5 mL THF and 37.5 mL acetone under

350 RPM agitation. 32 mL of water was charge to generate supersaturation, and 7 mg of seeds were added. 45 mL of water was charged over ~13 h. The slurry was isolated on a Buchner funnel, washed with 70 mL of 2:3 v:v acetone:water mix, and dried overnight at 70 ℃ in a vacuum oven.

Desupersaturation Measurements: Samples of supernatant were removed from the reactor at various time points during the seed age and antisolvent addition portions of the crystallization. Samples were filtered immediately with a 0.2 μm Whatman PTFE syringe filter, and diluted with 4:1 acetonitrile:water v:v for HPLC measurements. Concentration was determined via calibration of the HPLC (Shimadzu Scientific Instruments, Columbia MD) with samples of known concentration.

Particle Size Distribution (PSD) & Morphology Measurements: Optical microscopy (Axio Imager, Carl Zeiss Microscopy LLC, Thornwood, NY) was utilized to image the morphology of the particles in slurry. A Malvern Mastersizer 3000 (Malvern Panalytical, Malvern UK) equipped with the Scirocco 2000 accessory was used to measure the PSD of API samples for the one dimensional PBM. A dispersant pressure of 0.5 bar was used, the obscuration reading was in the range of 5 - 10 %, and three scans were conducted for each sample. The average value of the three separate sample measurements was used as the PSD input into the one dimensional PBM. For the PSD input into the two dimensional PBM, Malvern Morphologi G4 (Malvern Panalytical, Malvern UK) was utilized to measure the PSD of the major and minor axis separately. The samples were dispersed by gentle shaking in octane. The suspension was pipetted onto a microscope slide and dried. The batches were analyzed using a 20x magnification lens (1.8 – 100 micron resolution range).

PBM Construction: Solubility of Compound A was modelled with a hybrid polynomial/exponential equation. gPROMS Formulated Products Version 1.5 (gFP; PSE, London UK) was utilized for both 1D and 2D PBM. Errors associated with concentration and PSD measurements were described by a linear variance model as detailed in previous work.[30]

1D Model Construction: The 1D PBM was constructed utilizing the same workflow detailed in a previous work.[30] The three lab scale experiments were recreated *in silico*, through inputting the reactor configuration (reactor volume, impeller diameter, pumping number, and power number), the exact material charges, crystallization process steps (cooling rate, antisolvent addition rate), and experimental data (concentration of API in solution at various time points during the process, seed D10, D50, and D90, and final D10, D50, and D90) into gFP. Classical two-step growth[5] and Evans secondary nucleation[41] were selected to describe the crystallization mechanisms. gFP was utilized to estimate values for four parameters associated with the classical two-step growth equations (effective diffusivity correction factor, activation energy, growth rate constant, and supersaturation order) and three parameters associated with the Evans secondary nucleation rate equation (rate constant for crystal-impeller collisions, size above which crystals undergo attrition, and order with respect to supersaturation) to provide the best fit to the lab data.[30] The parameter values that provided the best fit were then utilized to predict desupersaturation when the process was run under different conditions via the GSA utility (see below).

2D Model Construction: Model construction followed a workflow similar to Ma et al.[19], and utilized a higher finite volume method to solve the population balance equation. The particle size quantiles (D10, D50, and D90) were inputted separately for the major and minor axis. Various crystallization mechanisms were investigated, and the associated parameters were

optimized to provide the best fit to the lab data. The mechanisms and associated parameter values that provided the best fit were then utilized to predict product aspect ratio when the process was run under different conditions via the GSA utility (see below).

Global Sensitivity Analysis (GSA): "Virtual DoEs" were conducted using the Global System Analysis capability within gFP, which predicts the effect of varying user-selected process parameters on properties of interest. For this work, the impact of agitation rate, seed load, seed PSD, seed point, or seed aspect ratio (AR) on desupersaturation and AR were predicted.

RESULTS AND DISCUSSION

The crystallization process generated needle-like crystals with length ranging from ~60-150 µm, and width of ~10-15 µm, as shown in Figure 1.

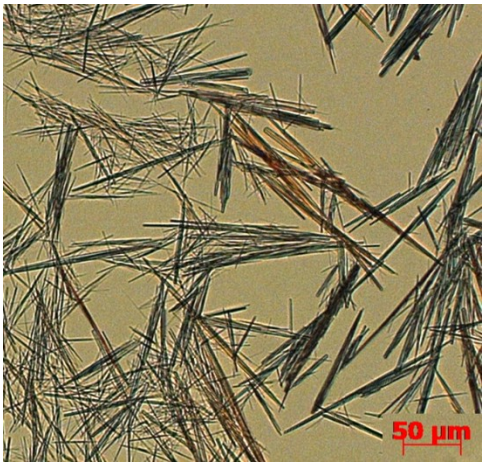

Figure 1. Optical microscope image of as-crystallized Compound A in slurry, at end of crystallization process.

These needle-like crystals exhibited poor powder properties, such as poor flowability and sticking. Additionally, the desupersaturation rate of the API from solution after addition of seeds was extremely slow (Figure 2) and the solubility concentration was not achieved even after ~50h

of aging. It is undesirable to proceed with the crystallization without complete desupersaturation, as entering the antisolvent addition step with a very high level of supersaturation results in poor control over the crystallization and increases the probability of large batch-to-batch PSD variance.[42] Thus, there was great interest in investigating process conditions that would enhance the degree of desupersaturation following seeding as well as reduce the particle aspect ratio (AR: ratio of particle length to width).

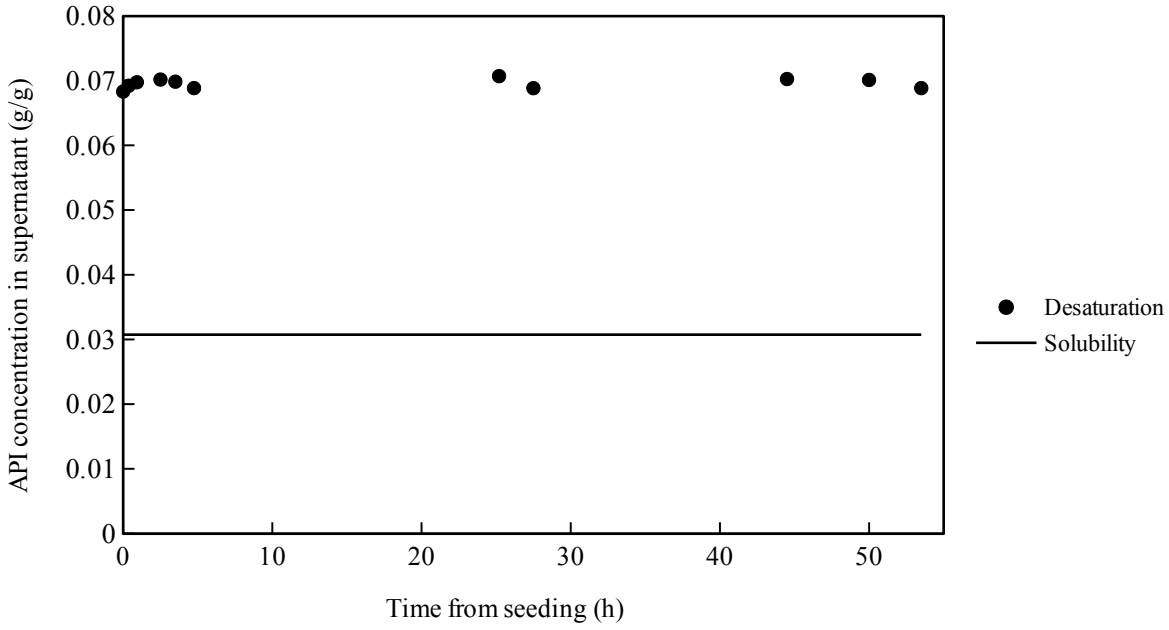

Figure 2. Concentration of Compound A in solution during crystallization process (Experiment 2), following seeding. After ~50 h of aging, the concentration is still far above the solubility, indicating incomplete desupersaturation.

The easier-to-construct 1D PBM was created initially, and used to guide further experimentation. However, before the 1D PBM could be made, a solubility model needed to be generated. The solubility data for Compound A was imported into gFP Utilities and was fit with a hybrid polynomial/exponential model. The measured solubility and corresponding modeled solubility

are shown in Figure 3. A one dimensional PBM was constructed utilizing the classical two step growth equations[5] and Evan's secondary nucleation equations[41]. Figure 4 shows the modeled API solution concentration (open circles) compared with the measured values (filled circles) and the solubility (dashed line) for experiments 1-3 (a-c, respectively).

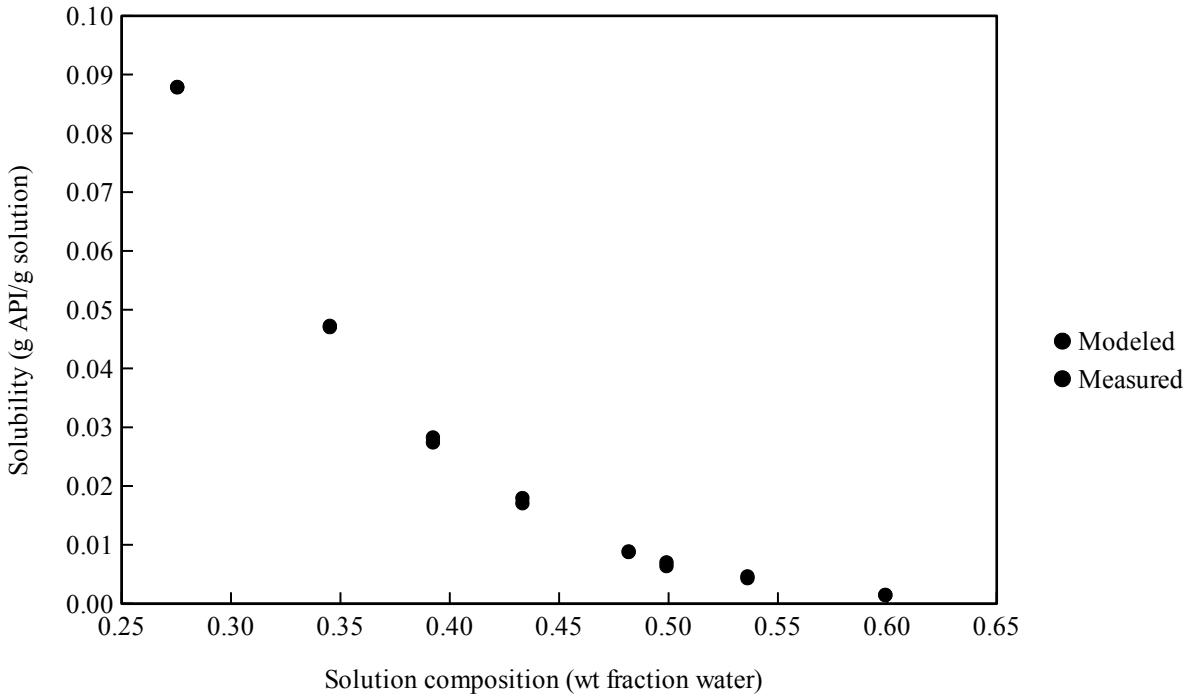

Figure 3. Measured solubility of Compound A (filled circles) and modeled solubility (empty circles). Due to the close overlap, the empty circles are not fully visible for most data points.

(a)

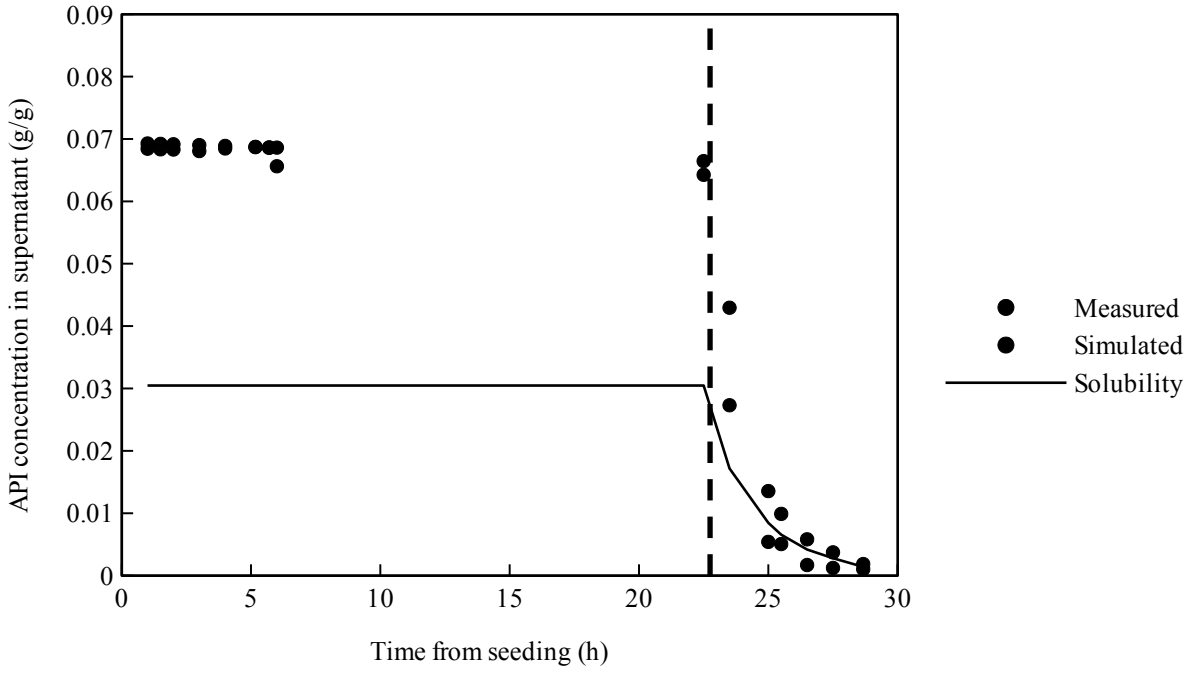
0.09
0.08
0.07
0.06
0.05
0.04
0.03
0.02
0.01
0
API concentration in supernatant (g/g)
0
5
10
15
20
25
30
Time from seeding (h)
Measured
Simulated
Solubility

(b)

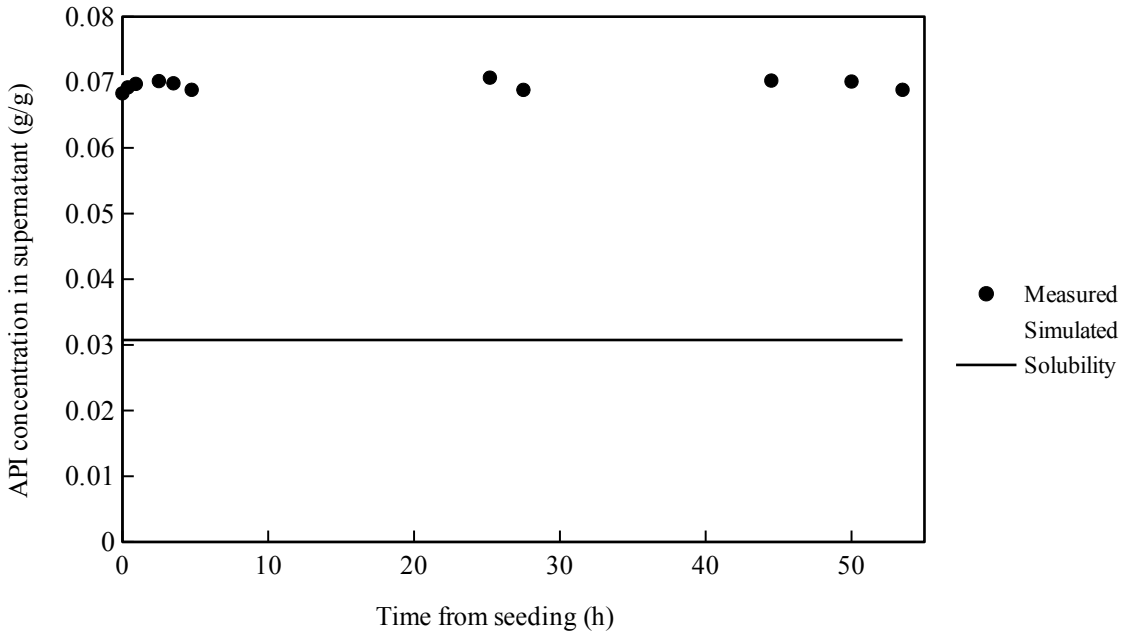
0.08
0.07
0.06
0.05
0.04
0.03
0.02
0.01
0
API concentration in supernatant (g/g)
0
10
20
30
40
50
Time from seeding (h)
Measured
Simulated
Solubility

(c)

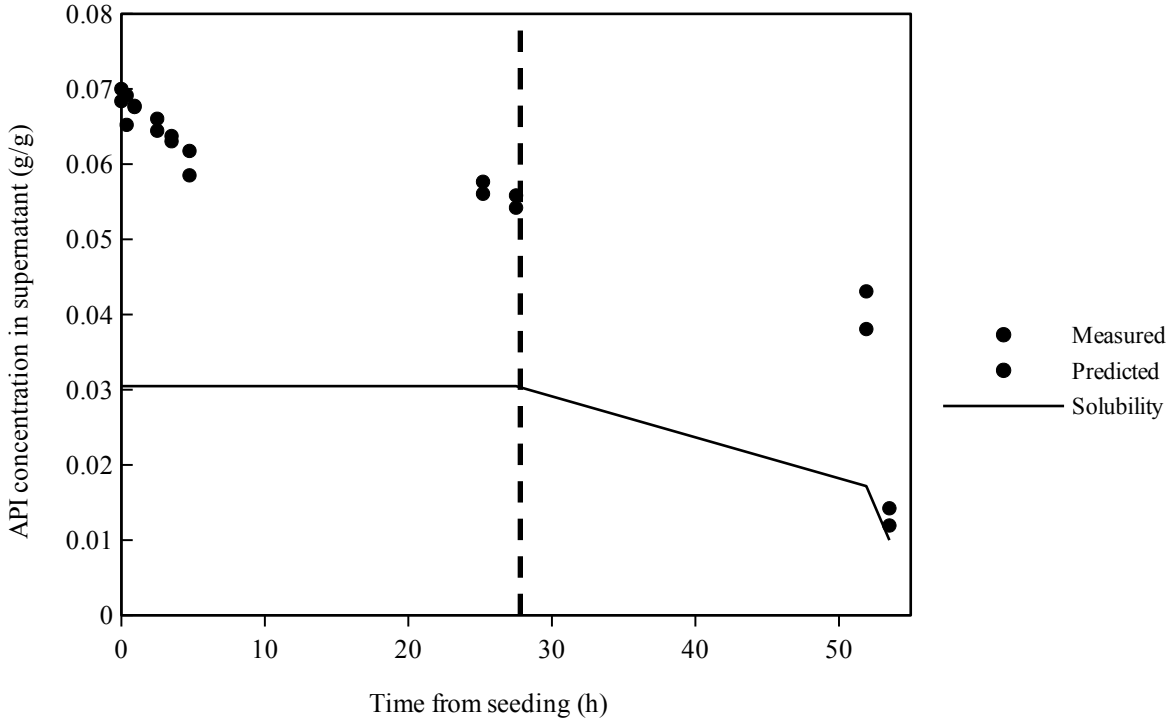
0.08
0.07
0.06
0.05
0.04
0.03
0.02
0.01
0
API concentration in supernatant (g/g)
0
10
20
30
40
50
Time from seeding (h)
Measured
Predicted
Solubility

Figure 4. Modeled API concentration (open circles) from 1D PBM compared to measured API concentration (closed circles) and solubility (dashed line) during the crystallization for crystallization experiments 1-3 (a-c, respectively).

The very small change observed in the desupersaturation data is due to the very slow desupersaturation of the API post-seeding. Desupersaturation to the solubility limit was only achieved during antisolvent addition, which is when the decrease in API concentration in solution is observed. The age time prior to antisolvent addition was varied between experiments, hence the plateau for the experiment in Figure 4(a) for experiment 1 is shorter than for that of Figure 4(c) for experiment 3. Desupersaturation data during the antisolvent addition phase were not collected for the crystallization in Figure 4(b), hence only the seed age portion is shown. The 1D PBM was then utilized to run virtual DOEs evaluating the effect of various crystallization process parameters on the API desupersaturation rate. The first process parameter investigated virtually was the impeller speed. If the slow desupersaturation rate was due to diffusion-limited growth, then enhancing the mixing should help to increase the rates of diffusion and, in turn, enhance the growth (and, correspondingly, the desupersaturation observed).[42] The impeller speed (modeled in a 250 mL Chemglass reactor) was found to have no impact on the desupersaturation (Figure 5). To verify the model predictions, a crystallization experiment at 550 RPM was conducted (Experiment 4), and found to provide no improvement to desupersaturation rate, as predicted by the model.

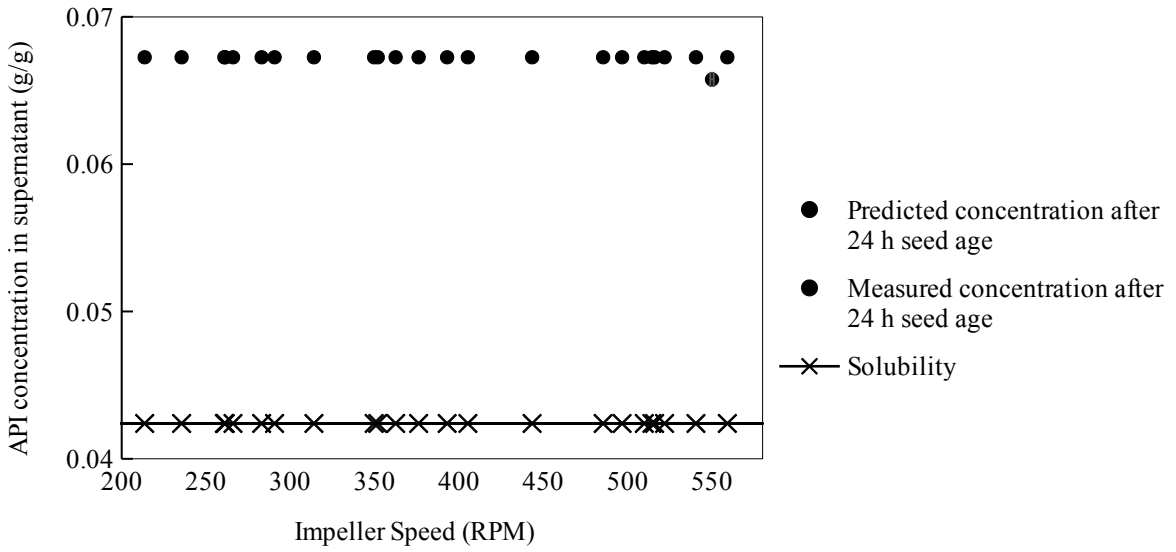

Figure 5. 1D PBM predicts no change in API concentration after 24 h of aging at different RPM; concentration is still much above the solubility concentration (indicated with line).

The impact of seed PSD and seed load on the desupersaturation rate was then investigated. Providing increased available surface area for growth via increasing seed load and/or decreasing seed PSD may enhance growth rate and desupersaturation.[43, 44] However, predictions from the 1D model indicated that increasing seed load to 10 wt % (Figure 6, black squares) provided only a minor enhancement to the API desupersaturation after 20 h of aging the slurry. Micronized seeds with small PSD (D90 = 15 μm; Figure 6, white squares) provided a small enhancement to desupersaturation as compared to standard seeds (D90 = 150 μm, black squares). Despite the small enhancement to the desupersaturation, the predicted concentration after 20 h was still significantly higher than the solubility (dashed line). An experiment with 10 wt % of jet milled seeds was conducted in the lab (experiment 5), and the API concentration in the supernatant (0.057 g/g) after ~20 h was within error of the model prediction.

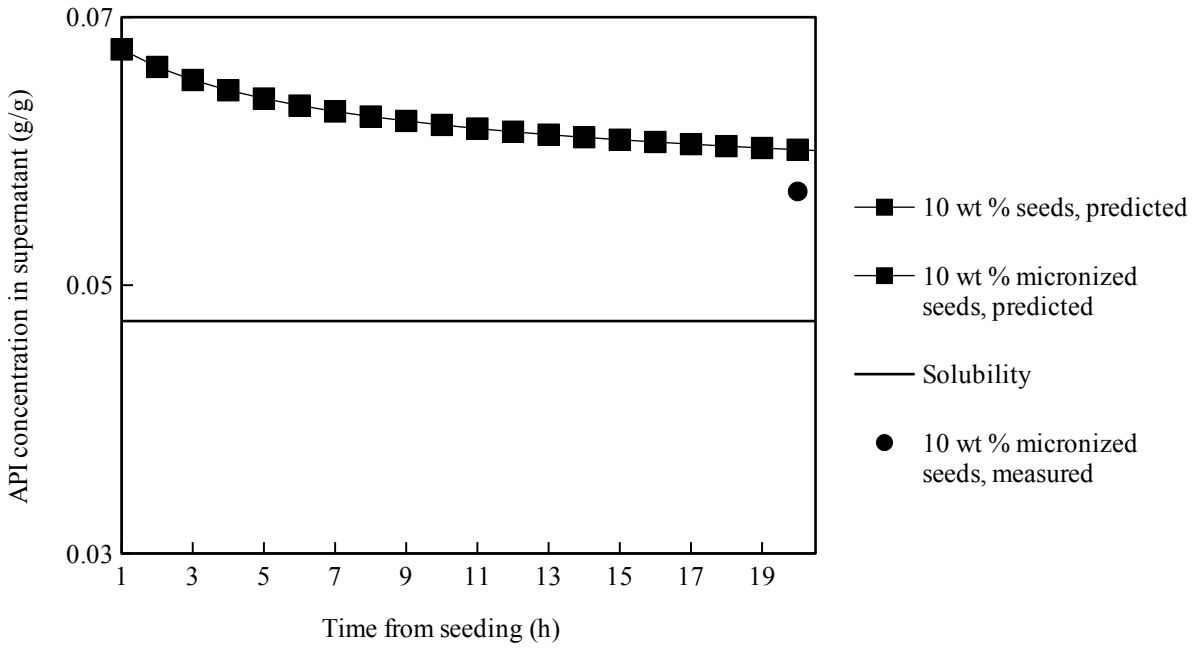

Figure 6. 1D PBM predictions of API concentration in supernatant during 20 h of age time following seeding for different seed loads and sizes (open shapes) compared to solubility (dashed line). Experimentally measured data point is indicated with filled circle.

The effect of supersaturation at the seed point on the desupersaturation rate was then investigated. Since supersaturation is the driving force for crystallization,[5] increasing the supersaturation should enhance the rate of crystallization (and desupersaturation). By altering the amount solvent and antisolvent relative to the API, the amount of supersaturation at the seed point can be varied. At the same API concentration, compositions with greater amounts of antisolvent will have lower API solubility and be more supersaturated. The supersaturation at seed point was found to greatly impact the API desupersaturation rate, as shown in Figure 7. The smallest degree of supersaturation occurs in the solution composition with the greatest solvent to antisolvent ratio. The greatest amount of supersaturation occurs in the composition with the lowest solvent to antisolvent ratio. .

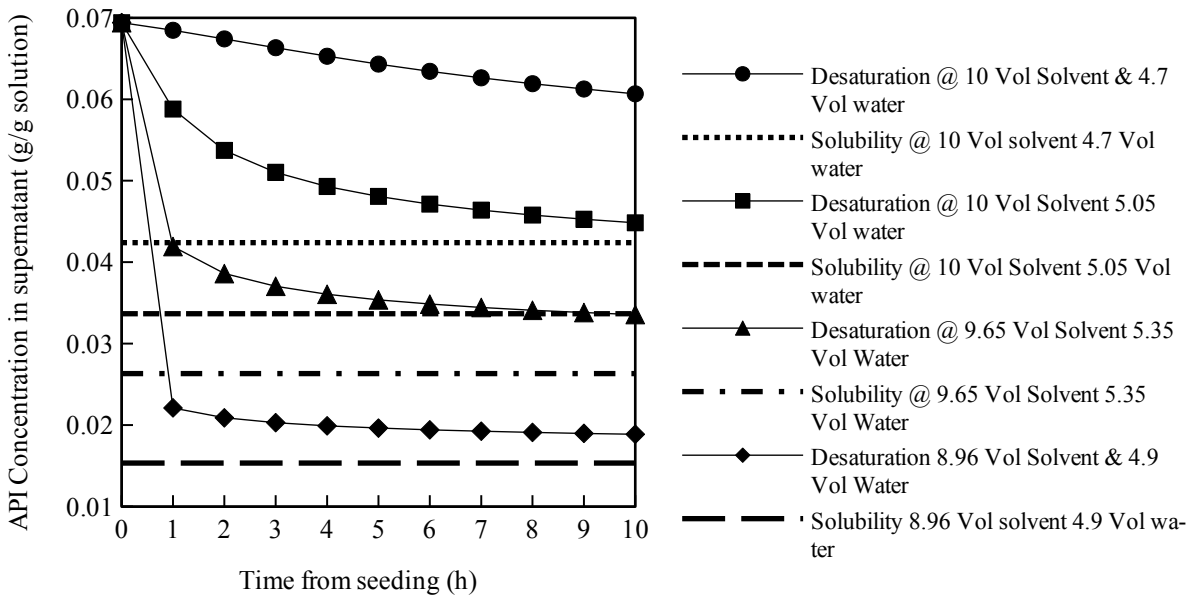

Figure 7. Predicted API desupersaturation rates from different seed point solution compositions and associated solubility. Volumes ("Vol") refers to processing volumes, which is a measurement of solution volume relative to API weight, and carries the unit of mL solution/g API.

The original seed point composition (10 Volumes solvent and 4.7 volumes water) exhibited slow desupersaturation. However, the 1D PBM model indicated that increasing the seed point supersaturation would greatly enhance the desupersaturation rate. Thus, a crystallization was conducted with the seed point at a higher supersaturation. This change allowed the process to rapidly desupersaturate and reach the solubility concentration after four h of aging as shown in Figure 8.

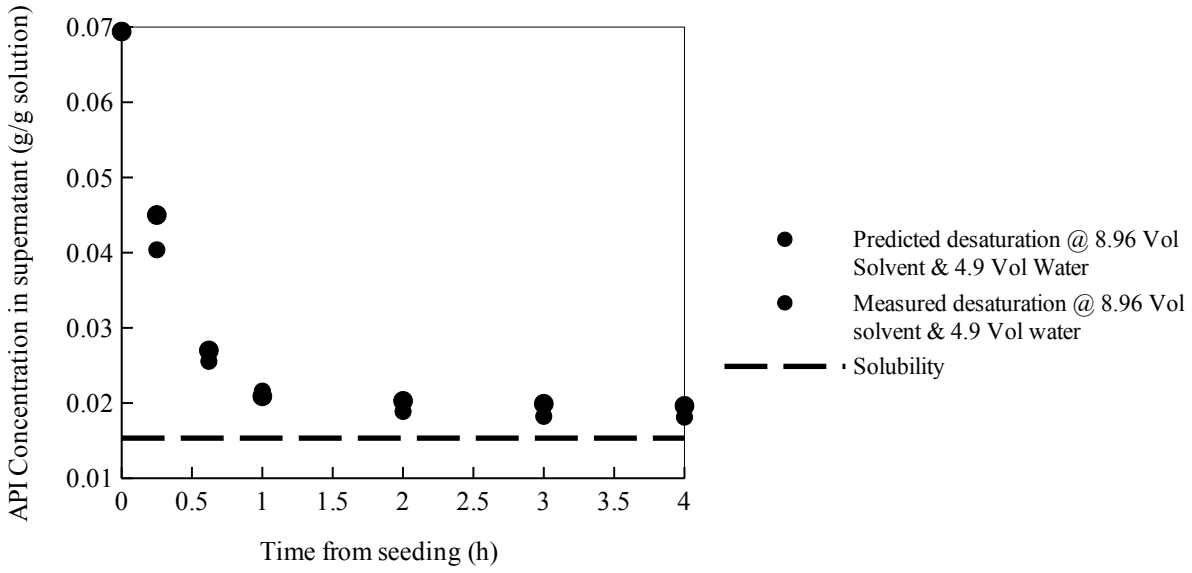

Figure 8. Measured API solution concentration (black circles) for Experiment 6 compared with predicted concentration (open circles) and solubility (dashed line).

While the 1D PBM was able to represent the API desupersaturation behavior, the model did not do well in matching the particle size quantiles. Figure 9 shows a parity plot comparing the simulated size quantiles to the measured quantiles. The poor fit is likely due to the isotropic growth assumption that is not valid for the high aspect ratio found in compound A's needle morphology. In order to improve the model fit to the PSD data, time was invested in constructing a 2D model.

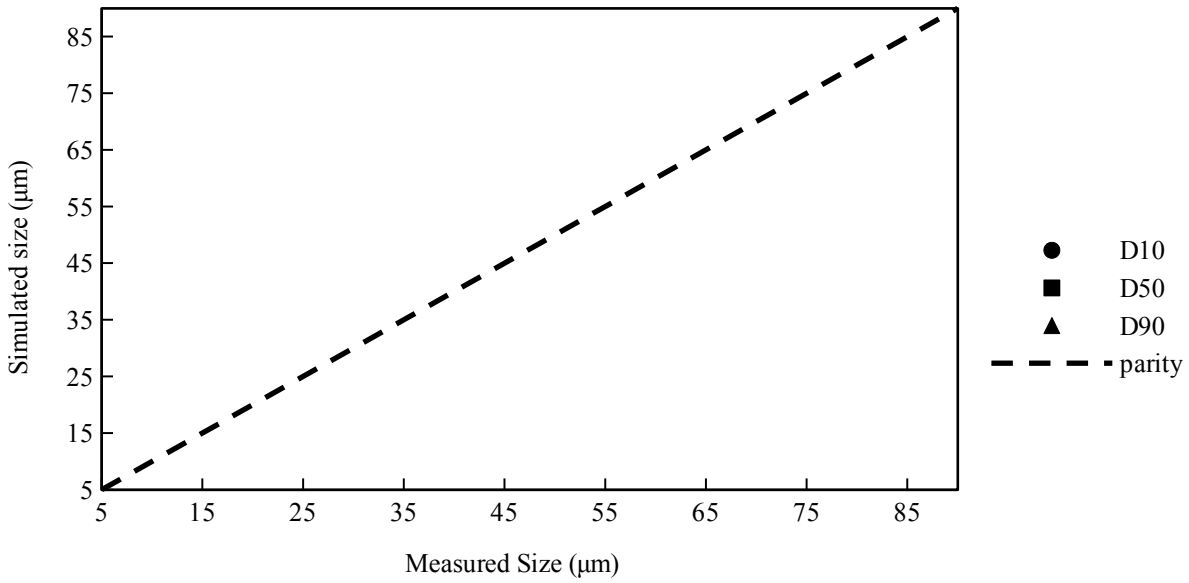

Figure 9. Parity plot of simulated size versus measured size quantiles (experiments 1-3) from one dimensional PBM; a perfect fit would lie on the parity line (dashed line).

While the same solubility model and seed PSD model prepared for the 1D model were utilized to construct the 2D model, separate major and minor axis size quantiles (obtained from Morphologi G3) were required for the 2D model. In the initial attempts at 2D model construction, the minor axis (needle diameter) growth rate was set as relative to the major axis (needle length) growth rate, with classical two-step growth utilized to describe growth rate kinetics. This approach did not provide a good match to the size data. Therefore, the major and minor axis growth rates were set as independent. The best fit to the measured API concentration and size quantile data was obtained utilizing a power law to describe growth, and Evan's secondary nucleation due to attrition[41]. Parameter estimation for the 2D model took on the order of days, whereas the 1D model only required a couple of hours. The fit of the 2D PBM to the API concentration data was very similar to that of the 1D PBM, and is thus not shown. The fit of the 2D PBM to the

measured major axis size quantiles is much improved over the 1D fit to the size data, as shown in Figure 10.

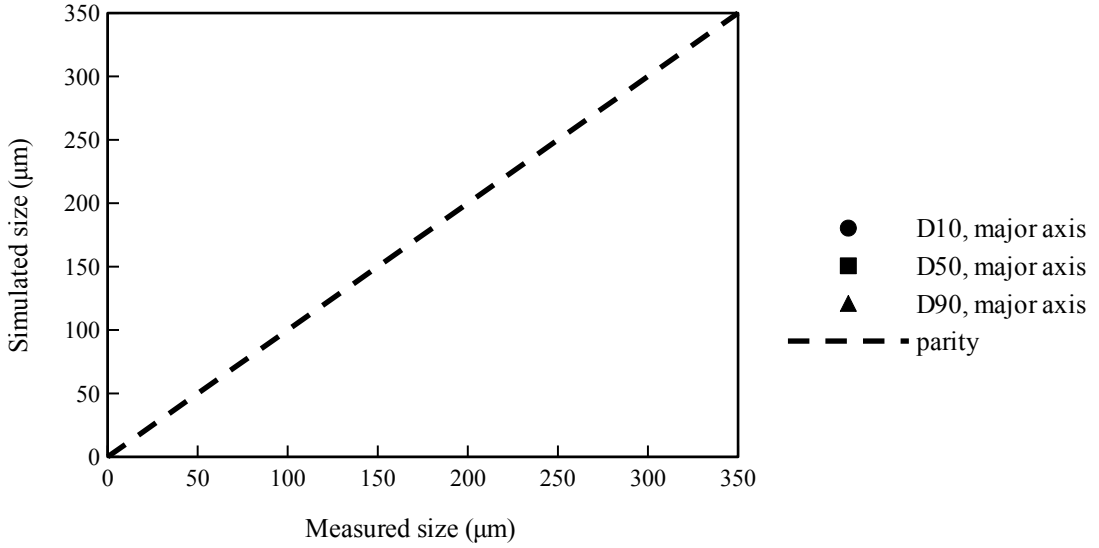

Figure 10. Comparison of simulated size from 2D PBM to measured major axis size quantiles for experiments 1-3.

After achieving a good fit to the particle size data, the 2D PBM was utilized to run virtual DOEs predicting the impact of various process parameters on the final particle aspect ratio. The impact of seed load with micronized seeds (D90 = 15 μm) on AR was investigated, as providing a lot of available surface area for growth may result in the particles growing more uniformly and reduce AR. As shown in Figure 11, extremely high seed loading was required to have any significant change to the aspect ratio of the final product. While such high seed loads are infeasible for production scale, a lab experiment with 25 wt % seed loading was conducted and verified the model predictions.

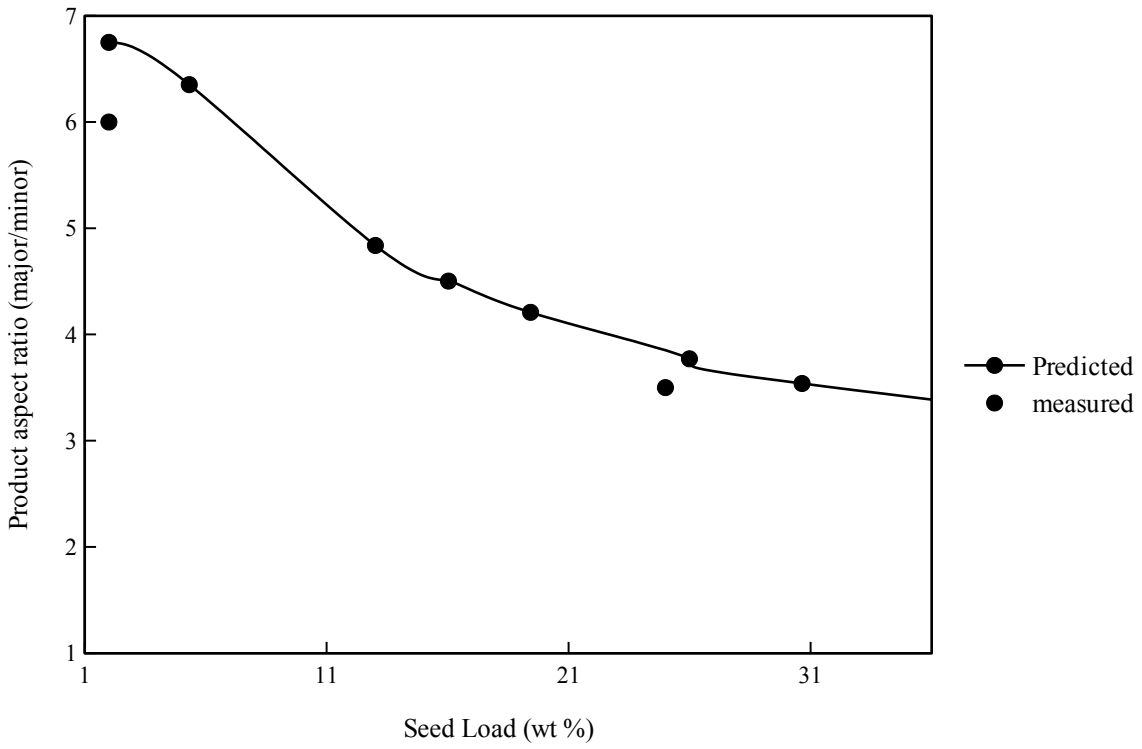

Figure 11. Prediction of aspect ratio versus seed load for micronized seeds, and experimentally measured points (black circles; Experiments 3 & 7).

Another common seed-based strategy to encourage growth of more equant shaped (low aspect ratio) particles is to utilize equant seeds. It is sometimes possible to generate a small amount of low aspect ratio particles for seed material via a methodology that is not amenable to scale-up (e.g. from a high throughput plate-based screening, or via a carefully controlled temperature cycle process). The rationale behind this approach is that the equant seeds serve as a template for more uniform growth. Therefore, the 2D PBM was utilized to predict the impact of seed aspect ratio on the aspect ratio of the final material across a range of seed loadings (Figure 12).

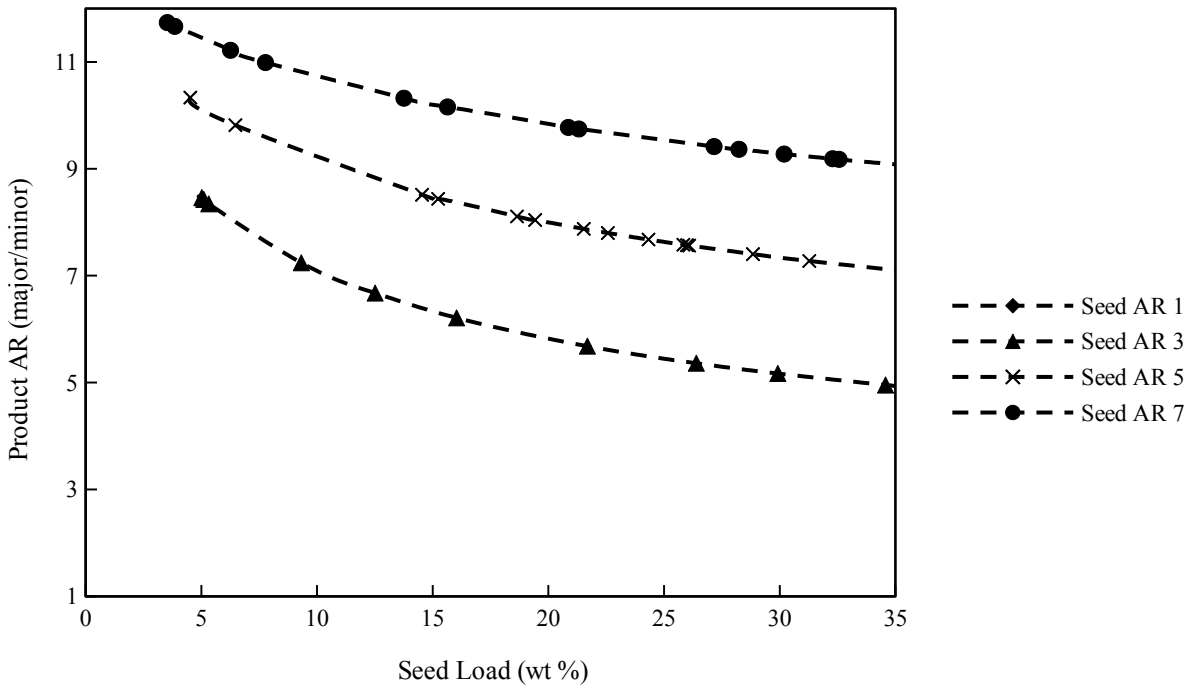

Figure 12. Prediction of the effect of seed aspect ratio and loading on the AR of the resulting material.

As seen in Figure 12, the 2D PBM predicts that even with perfectly symmetrical morphology seeds (cubes/spheres, AR 1), a high seed loading (> 10 wt %) is needed to generate lower AR final material. On the basis of the model predictions, another morphology for use as seeds was not pursued.

Lastly, in some cases slowing the rate of antisolvent addition can provide a more equant morphology by allowing the slow growth direction (minor axis) an opportunity to grow.[45-47] The 2D PBM was utilized to predict the product AR throughout the crystallization for three different antisolvent addition rates (following a 6 h post-seeding slurry age period). As seen in Figure 13, the AR rapidly increases very early in the antisolvent addition, even with extremely slow (24 h) addition. These simulations indicated that slowing the antisolvent addition rate would not

generate particles with significantly lower aspect ratio. An experiment with a 13 h antisolvent addition (experiment 8) generated particles with average aspect ratio 10.5 (compared to average AR ~11.5 for 6 h antisolvent addition; experiments 1-3) confirming this behaviour.

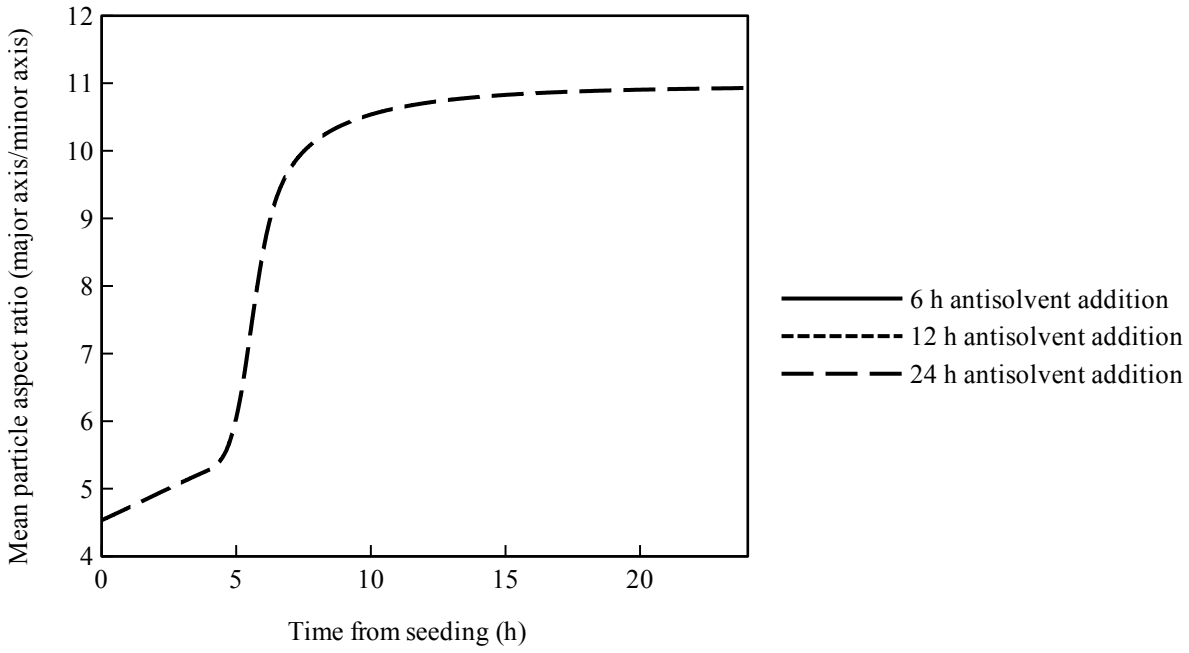

Figure 13. Simulations of the product aspect ratio throughout the crystallization process for three different antisolvent addition rates.

CONCLUSIONS

A 1D and a 2D PBM were constructed to model a crystallization process that both exhibited slow desupersaturation following seeding and generated particles with needle-like morphology. While the 1D model was faster to construct computationally and required less input data, the model had limited utility because of its poor matching of particle size data. The 1D model was able to match the in-process API concentration data and thus was useful for running virtual DOEs to predict the impact of different crystallization process parameters on the desupersaturation rate. These predictions ultimately were able to resolve the slow

desupersaturation challenge by focusing the lab work on the most influential process parameter – supersaturation at seeding. However, the more data and computationally intensive 2D PBM was needed to model the particle size data. The 2D model had a good fit to the major axis quantiles (particle length) and was utilized to predict impact of crystallization process parameters on the particle AR. The predictions indicated that the final particles would have high AR even with equant (sphere or cube shaped) seeds or an extremely slow (24 h) antisolvent addition rate, rendering it unlikely to achieve reduction of the particle aspect ratio through optimization of the crystallization process alone.

ACKNOWLEDGEMENTS

The authors gratefully acknowledge B. Seifried for providing a critical review of the manuscript.

REFERENCES

1. Cote, A.; Erdemir, D.; Girard, K. P.; Green, D. A.; Lovette, M. A.; Sirota, E.; Nere, N. K., Perspectives on the Current State, Challenges, and Opportunities in Pharmaceutical Crystallization Process Development. *Crystal Growth & Design* **2020,** *20* (12), 7568-7581.

2. Trampuž, M.; Teslić, D.; Likozar, B., Process analytical technology-based (PAT) model simulations of a combined cooling, seeded and antisolvent crystallization of an active pharmaceutical ingredient (API). *Powder Technology* **2020,** *366*, 873-890.

3. Variankaval, N.; Cote, A.; Doherty, M., From Form to Function: Crystallization of Active Pharmaceutical Ingredients. *AIChE Journal* **2008,** *54* (7), 1682-1688.

4. Mitchell, N. A.; Ó'Ciardhá, C. T.; Frawley, P. J., Estimation of the growth kinetics for the cooling crystallisation of paracetamol and ethanol solutions. *Journal of Crystal Growth* **2011,** *328* (1), 39-49.

5. Myerson, A. S.; Ginde, R., 2 - Crystals, crystal growth, and nucleation. In *Handbook of Industrial Crystallization (Second Edition)*, Myerson, A. S., Ed. Butterworth-Heinemann: Woburn, 2002; pp 33-65.

6. Costa, C. B. B.; Maciel, M. R. W.; Filho, R. M., Considerations on the crystallization modeling: Population balance solution. *Computers & Chemical Engineering* **2007,** *31* (3), 206-218.

7. Liu, Y. C.; Acevedo, D.; Yang, X.; Naimi, S.; Wu, W.-L.; Pavurala, N.; Nagy, Z. K.; O'Connor, T. F., Population Balance Model Development Verification and Validation of Cooling Crystallization of Carbamazepine. *Crystal Growth & Design* **2020,** *20* (8), 5235-5250.

8. Briesen, H., Simulation of crystal size and shape by means of a reduced two-dimensional population balance model. *Chemical Engineering Science* **2006,** *61* (1), 104-112.

9. Sato, K.; Nagai, H.; Hasegawa, K.; Tomori, K.; Kramer, H. J. M.; Jansens, P. J., Two-dimensional population balance model with breakage of high aspect ratio crystals for batch crystallization. *Chemical Engineering Science* **2008,** *63* (12), 3271-3278.

10. Zhang, Y.; Doherty, M. F., Simultaneous prediction of crystal shape and size for solution crystallization. *AIChE Journal* **2004,** *50* (9), 2101-2112.

11. Zhang, Y.; Liu, J. J.; Wan, J.; Wang, X. Z., Two dimensional population balance modelling of crystal growth behaviour under the influence of impurities. *Advanced Powder Technology* **2015,** *26* (2), 672-678.

12. Muthancheri, I.; Long, B.; Ryan, K. M.; Padrela, L.; Ramachandran, R., Development and validation of a two-dimensional population balance model for a supercritical CO2 antisolvent batch crystallization process. *Advanced Powder Technology* **2020,** *31* (8), 3191-3204.

13. Puel, F.; Févotte, G.; Klein, J. P., Simulation and analysis of industrial crystallization processes through multidimensional population balance equations. Part 2: a study of semi-batch crystallization. *Chemical Engineering Science* **2003,** *58* (16), 3729-3740.

14. Shoji, M.; Takiyama, H., The Application of Two-Dimensional Population Balance Model To Study the Effect of Temperature Profile on the Crystal Size Distribution and Aspect Ratio. *Crystal Growth & Design* **2012,** *12* (11), 5241-5246.

15. Liu, J. J.; Ma, C. Y.; Hu, Y. D.; Wang, X. Z., Modelling protein crystallisation using morphological population balance models. *Chemical Engineering Research and Design* **2010,** *88* (4), 437-446.

16. Qian, Y.; Lu, G.; Sun, Y.; Song, X.; Yu, J., Modeling of strontium chloride hexahydrate growth during unseeded batch cooling crystallization by two-dimensional population balance equation. *CrystEngComm* **2015,** *17* (48), 9394-9403.

17. Ma, C. Y.; Wang, X. Z., Model identification of crystal facet growth kinetics in morphological population balance modeling of L-glutamic acid crystallization and experimental validation. *Chemical engineering science* **2012,** *70*, 22-30.

18. Ma, C. Y.; Wang, X. Z.; Roberts, K. J., Multi-dimensional population balance modeling of the growth of rod-like L-glutamic acid crystals using growth rates estimated from in-process imaging. *Advanced Powder Technology* **2007,** *18* (6), 707-723.

19. Ma, C. Y.; Wang, X. Z.; Roberts, K. J., Morphological population balance for modeling crystal growth in face directions. *AIChE journal* **2008,** *54* (1), 209-222.

20. Liu, J. J.; Ma, C. Y.; Hu, Y. D.; Wang, X. Z., Effect of seed loading and cooling rate on crystal size and shape distributions in protein crystallization—a study using morphological population balance simulation. *Computers & Chemical Engineering* **2010,** *34* (12), 1945-1952.

21. Oullion, M.; Puel, F.; Févotte, G.; Righini, S.; Carvin, P., Industrial batch crystallization of a plate-like organic product. In situ monitoring and 2D-CSD modelling. Part 2: Kinetic modelling and identification. *Chemical Engineering Science* **2007,** *62* (3), 833-845.

22. Ma, C. Y.; Wang, X. Z., Crystal growth rate dispersion modeling using morphological population balance. *AIChE Journal* **2008,** *54* (9), 2321-2334.

23. Kodera, T.; Kobari, M.; Hirasawa, I., Modeling and Growth Kinetics of Antisolvent Crystallization Applied to the Pharmaceutical Industry. *Chemical Engineering & Technology* **2019,** *42* (7), 1458-1465.

24. Vetter, T.; Iggland, M.; Ochsenbein, D. R.; Hänseler, F. S.; Mazzotti, M., Modeling nucleation, growth, and Ostwald ripening in crystallization processes: a comparison between population balance and kinetic rate equation. *Crystal growth & design* **2013,** *13* (11), 4890-4905.

25. Shu, Y. D.; Liu, J. J.; Zhang, Y.; Wang, X. Z., A multi-stage multi-component transfer rate morphological population balance model for crystallization processes. *CrystEngComm* **2019,** *21* (28), 4212-4220.

26. Nagy, Z.; Aamir, E.; Rielly, C., Internal fines removal using population balance model based control of crystal size distribution under dissolution, growth and nucleation mechanisms. *Crystal growth & design* **2011,** *11* (6), 2205-2219.

27. Ridder, B. J.; Majumder, A.; Nagy, Z. K., Population balance model-based multiobjective optimization of a multisegment multiaddition (MSMA) continuous plug-flow antisolvent crystallizer. *Industrial & Engineering Chemistry Research* **2014,** *53* (11), 4387-4397.

28. Oucherif, K. A.; Raina, S.; Taylor, L. S.; Litster, J. D., Quantitative analysis of the inhibitory effect of HPMC on felodipine crystallization kinetics using population balance modeling. *CrystEngComm* **2013,** *15* (12), 2197-2205.

29. Caillet, A.; Sheibat-Othman, N.; Fevotte, G., Crystallization of monohydrate citric acid. 2. Modeling through population balance equations. *Crystal Growth & Design* **2007,** *7* (10), 2088-2095.

30. Rosenbaum, T.; Tan, L.; Dummeldinger, M.; Mitchell, N.; Engstrom, J., Population Balance Modeling To Predict Particle Size Distribution upon Scale-Up of a Combined Antisolvent and Cooling Crystallization of an Active Pharmaceutical Ingredient. *Organic Process Research & Development* **2019,** *23* (12), 2666-2677.

31. Woo, X. Y.; Tan, R. B.; Braatz, R. D., Modeling and computational fluid dynamics− population balance equation− micromixing simulation of impinging jet crystallizers. *Crystal Growth and Design* **2009,** *9* (1), 156-164.

32. Fu, X.; Zhang, D.; Xu, S.; Yu, B.; Zhang, K.; Rohani, S.; Gong, J., Effect of Mixing on the Particle Size Distribution of Paracetamol Continuous Cooling Crystallization Products Using a Computational Fluid Dynamics–Population Balance Equation Simulation. *Crystal Growth & Design* **2018,** *18* (5), 2851-2863.

33. Nagy, Z. K., Model based robust control approach for batch crystallization product design. *Computers & Chemical Engineering* **2009,** *33* (10), 1685-1691.

34. Lindenberg, C.; Krättli, M.; Cornel, J.; Mazzotti, M.; Brozio, J. r., Design and optimization of a combined cooling/antisolvent crystallization process. *Crystal Growth and Design* **2009,** *9* (2), 1124-1136.

35. Abbas, A.; Romagnoli, J. A., Multiscale modeling, simulation and validation of batch cooling crystallization. *Separation and Purification Technology* **2007,** *53* (2), 153-163.

36. Czapla, F.; Haida, H.; Elsner, M.; Lorenz, H.; Seidel-Morgenstern, A., Parameterization of population balance models for polythermal auto seeded preferential crystallization of enantiomers. *Chemical engineering science* **2009,** *64* (4), 753-763.

37. Iggland, M.; Mazzotti, M., Population balance modeling with size-dependent solubility: Ostwald ripening. *Crystal growth & design* **2012,** *12* (3), 1489-1500.

38. Worlitschek, J.; Mazzotti, M., Model-based optimization of particle size distribution in batch-cooling crystallization of paracetamol. *Crystal Growth & Design* **2004,** *4* (5), 891-903.

39. Li, H.; Kawajiri, Y.; Grover, M. A.; Rousseau, R. W., Modeling of nucleation and growth kinetics for unseeded batch cooling crystallization. *Industrial & Engineering Chemistry Research* **2017,** *56* (14), 4060-4073.

40. Zhang, H.; Quon, J.; Alvarez, A. J.; Evans, J.; Myerson, A. S.; Trout, B., Development of continuous anti-solvent/cooling crystallization process using cascaded mixed suspension, mixed product removal crystallizers. *Organic Process Research & Development* **2012,** *16* (5), 915-924.

41. Evans, T. W.; Sarofim, A. F.; Margolis, G., Models of secondary nucleation attributable to crystal-crystallizer and crystal-crystal collisions. *AIChE Journal* **1974,** *20* (5), 959-966.

42. Singh, U. K.; Pietz, M. A.; Kopach, M. E., Identifying Scale Sensitivity for API Crystallizations from Desupersaturation Measurements. *Organic Process Research & Development* **2009,** *13* (2), 276-279.

43. Long, B.; Yang, H.; Ding, Y., Impact of seed loading ratio on the growth kinetics of mono-ammonium phosphate under isothermal batch crystallization. *Korean journal of chemical engineering* **2016,** *33* (2), 623-628.

44. Choi, J. Y.; Lee, T.; Cheng, Y.; Cohen, Y., Observed Crystallization Induction Time in Seeded Gypsum Crystallization. *Industrial & Engineering Chemistry Research* **2019,** *58* (51), 23359-23365.

45. Croker, D. M.; Kelly, D. M.; Horgan, D. E.; Hodnett, B. K.; Lawrence, S. E.; Moynihan, H. A.; Rasmuson, Å. C., Demonstrating the Influence of Solvent Choice and Crystallization Conditions on Phenacetin Crystal Habit and Particle Size Distribution. *Organic Process Research & Development* **2015,** *19* (12), 1826-1836.

46. Kim, D.-C.; Yeo, S.-D., Habit modification of tamoxifen crystals using antisolvent crystallizations. *Korean Journal of Chemical Engineering* **2017,** *34* (5), 1466-1474.

47. Tiwary, A. K., Modification of Crystal Habit and Its Role in Dosage Form Performance. *Drug Development and Industrial Pharmacy* **2001,** *27* (7), 699-709.